Edgemap-Based Wiener Filtering for Preserving Image Fine Details and Edges

SUHAILA SARI and TETSUYA SHIMAMURA
Graduate School of Science and Engineering
Saitama University
Shimo-Okubo 255, Sakura-ku, Saitama, 338-8570
JAPAN
{suhaila, shima}@sie.ics.saitama-u.ac.jp

Abstract: - In this paper, we present a denoising technique that is capable for preserving the fine details and edges in the restored image more effectively in blind condition. We also introduce a new edge detection method to detect edges effectively in noisy environments. First, the noisy image is denoised by using different weights of Wiener filtering to generate two restored images; one with highly reduced noise, and the other with preserved fine details and edges. The noise and image power spectra required for the frequency domain Wiener filter are estimated with different threshold setting. Then, an edgemap image is generated directly from the noisy image. The two Wiener filtered images are utilized for the smooth and non-smooth regions based on the constructed edgemap to produce the final restored image. Simulation results show that the proposed method outperforms or is comparable to other Wiener filter-based denoising methods and the state-of-the-art denosing methods, especially in higher noise environments.

Key-Words: - Edgemap, Edge detection, Image denoising, Power spectrum estimation, Wiener filter

1 Introduction

Although image denoising has been researched quite extensively, developing a denoising method that could remove noise effectively without eliminating the image fine details and edges is still a challenging task. Until recent years, many denoising methods have been proposed. Some recent non-linear methods, such as the adaptive Total Variation (ATV) [1] and the non-local means (NLM) [2], suggest employing different denoising approaches for the smooth and non-smooth regions. Conversely, linear methods such as the Wiener filter [3] balance the tradeoff between inverse filtering and noise smoothing by eliminating additive noise while inverting blurring.

The Wiener filter is the best-known technique for the linear image denoising. It has been implemented for image denoising in several transform domains, for example the spatial domain [4] and the frequency domain [5]. Recently, the wavelet-based denoising methods have dominated the latest research trend in image processing. The implementation of the Wiener filter in the wavelet domain has also been introduced, for example the lifting-based wavelet domain Wiener filter (LBWDWF) [6]. However, to utilize the Wiener filter in practical cases, where the information of the original image and the noise level are unknown (blind condition), noise estimation plays an important role to accomplish accurate denoising. The ATV derives the idea of the Total Variation (TV) [7]. The ATV reduces the total variation of the image adaptively. It employs strong denoising in the smooth regions and weak denoising in the non-smooth regions. The NLM measures the similarity of the grey level between two pixels and compares the geometrical configuration adapted to the local and non-local geometry of the whole image. The methods such as the LBWDWF, ATV and NLM are reported to have superior performance in noise removal and preservation of strong edges. They, however, share a common drawback: that is, the fine details and edges of the original image are not well preserved in the restored image, especially in higher noise environments.

To overcome this problem, a frequency domain Wiener filter-based denoising has been proposed in [8]. We refer this method to as the frequency domain Wiener filter (FDWF). It introduces a noise and image power spectra estimation method for the implementation of the Wiener filter in blind condition. The FDWF provides the preservation of the fine details and edges, but a certain level of noise still remains in the restored image.

In this paper, we propose a denoising technique that is based on the FDWF. The image restored by using the FDWF with a lower threshold value is utilized in the non-smooth regions in the final restored image. Conversely, the image restored by

using the FDWF with a higher threshold value is employed in the smooth regions in the final restored image. A new edge detection method is employed to distinguish between the smooth and non-smooth regions effectively in the presence of noise. The edge detection is performed in four directions and the results are combined to construct an edgemap. The final restored image is constructed by assigning the smooth and non-smooth regions based on the edgemap. Simulation results verify a significant reduction of the noise level in the smooth regions relative to that of the FDWF.

The paper is organized as follows. We begin with the introduction of the FDWF in Section 2, and then describe the proposed denoising method in Section 3. In Section 4, we discuss the simulation results and the performance comparison of our method. In Section 5, we draw concluding remarks.

2 FDWF

Our procedure for image denoising utilizes the FDWF proposed in [8]. We assume that the image is corrupted by independent additive zero-mean Gaussian white noise. A noisy image, $p(u,v)$, corrupted by the noise, $n(u,v)$, can be expressed as

$$p(u,v) = h(u,v) + n(u,v) \tag{1}$$

where $h(u,v)$ represents the original image. The FDWF employs a threshold process to estimate the image and noise power spectra. The assumption is that in general, the noise power spectrum usually occupies high frequencies, and conversely the image power spectrum is commonly concentrated at low frequencies.

First, we transform the noisy image $h(u,v)$ to the frequency domain, $\hbar(s,t)$, by using the FFT. The power spectrum of $\hbar(s,t)$, $H(s,t)$, is obtained by

$$H(s,t) = |\hbar(s,t)|^2 \tag{2}$$

and the logarithmic power spectrum of $H(s,t)$, $G(s,t)$, is given by

$$G(s,t) = log\,(H(s,t)). \tag{3}$$

We perform the estimation for the power spectra of the image and noise block-by-block. $H(s,t)$ and $G(s,t)$ are divided into $k\times k$ non-overlapping sub-blocks. $H_{(i,j)}(s,t)$ and $G_{(i,j)}(s,t)$ correspond to the (i,j)th block of $H(s,t)$ and $G(s,t)$, respectively. Next, we compute the average of the logarithmic power spectrum in each $G_{(i,j)}(s,t)$ sub-block, which is denoted as $\overline{G}_{(i,j)}(s,t)$, respectively. We find from all the image's sub-blocks the $\overline{G}_{(i,j)}(s,t)$ that represent the median and minimum values of the entire $\overline{G}_{(i,j)}(s,t)$. The minimum value, $\overline{G}\_min$, and the maximum value, $\overline{G}\_med$, are substituted in the following global threshold value as

$$\alpha = \overline{G}\_med \cdot \frac{\lambda}{100} + \overline{G}\_min \tag{4}$$

where λ denotes a division ratio of $\overline{G}\_med$, and α corresponds to the threshold used for the power spectrum estimation.

The utilization of $\overline{G}\_med$ in (4) is attributed to the fact that the median represents where most of the power spectrum are concentrated. If the division of the high and low frequencies considers the main power concentration, the threshold value will be more robust to the variation of the power spectrum characteristics in different images. The threshold value is set to be slightly higher than $\overline{G}\_min$ to avoid the probability of the noise power spectrum being incorrectly thresholded into the image power spectrum. In (4), λ is utilized to adjust the threshold range.

The noise power spectrum is estimated from both high and low frequency regions, since we consider that the noise occupies both regions. In high frequency region, the image power spectrum, $P_{(i,j)}(s,t)$, and the noise power spectrum, $N_{(i,j)}(s,t)$, in the corresponding sub-block are approximated by

$$\begin{aligned} &\text{if} \quad \overline{G}_{(i,j)}(s,t) \le \alpha, \\ &\text{then} \ P_{(i,j)}(s,t) = 0,\ N_{(i,j)}(s,t) = H_{(i,j)}(s,t). \end{aligned} \tag{5}$$

In low frequency region, $P_{(i,j)}(s,t)$ and $N_{(i,j)}(s,t)$ are estimated as

$$\begin{aligned} &\text{if} \quad \overline{G}_{(i,j)}(s,t) > \alpha, \\ &\text{then} \ P_{(i,j)}(s,t) = H_{(i,j)}(s,t), \\ &\mathrm{N}_{(i,j)}(s,t) = \text{average}\,[\,H_{(0,0)}(s,t), H_{(0,k-1)}(s,t), \\ &\qquad\qquad H_{(k-1,0)}(s,t), H_{(k-1,k-1)}(s,t)] \end{aligned} \tag{6}$$

where the average $[\cdots]$ represents the averaging of the sub-blocks in the four corners being at the highest frequencies. These four blocks are assumed to be occupied only by noise. Fig.1 demonstrates the described four corners in the case of k=8.

Finally, we perform the Wiener filtering operation. The Wiener filter, $W(s,t)$, is obtained by

$$W(s,t) = \frac{P_{(i,j)}(s,t)}{P_{(i,j)}(s,t) + N_{(i,j)}(s,t)}. \tag{7}$$

ISBN: 978-1-61804-023-7

In [8], the parameters k and λ are set to be 32 and 5, respectively. This is due to that when λ=5, it provides a robust and optimal restoration result for the FDWF in different image characteristics and noise levels. When λ is fixed to be lower (for example λ =5), the threshold range will be larger. This setting will include higher frequencies in the estimated image power spectrum. This will contribute to the preservation of the image fine details and edges that usually occupy higher frequencies. Fig.2 shows the close-up view of the restored Cameraman image and its logarithmic power spectrum (corrupted by the white noise with the standard deviation, σ, of 25) by using the FDWF with λ=5. From Fig. 2 we can observe that the FWDF has preserved fine details and edges successfully, but has not effectively eliminated the noise in the restored image.

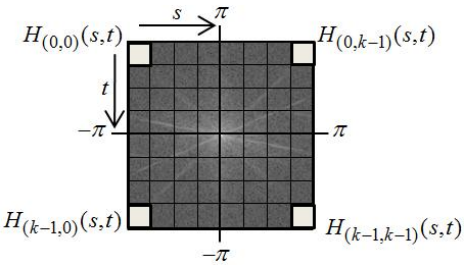

Fig.1 Average of four corners (highest frequencies).

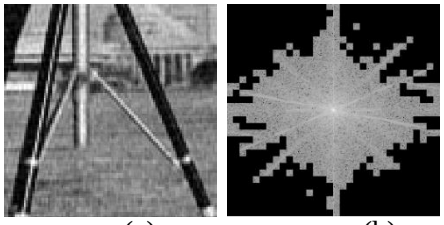

(a) (b)

Fig.2 Restored Cameraman and its logarithmic power spectrum (σ=25) by using FDWF (λ =5).

3 Proposed Algorithm

The method proposed in this paper reduces the noise in the image restored by using the FDWF with different parameters in the smooth and non-smooth regions. From our investigation, narrower threshold range setting in the FDWF reduces noise level, and larger threshold range setting preserves the fine details and edges. We set out to improve the FDWF restoration performance by utilizing the advantage of both threshold settings. Fig.3 shows a block diagram of our method.

3.1 Image Restoration for Non-Smooth Regions

The image restored by the FDWF with λ=5 is inverse-transformed to the spatial domain and represented as $f\_5(u,v)$ hereafter. The $f\_5(u,v)$ is utilized for the non-smooth regions in the final restored image, since it preserves the fine details and edges effectively.

3.2 Image Restoration for Smooth Regions

Conversely, an image with highly reduced noise, which is restored by using the FDWF with higher λ setting, is employed for the smooth regions in the final restored image. If λ is set to be higher, the threshold range of λ will be narrower. This will allow the FDWF to threshold only the concentrated part of the low frequencies, which is assumed to be occupied only by the image power spectrum.

First, the most suitable λ setting that provides a restored image with considerably low noise level is

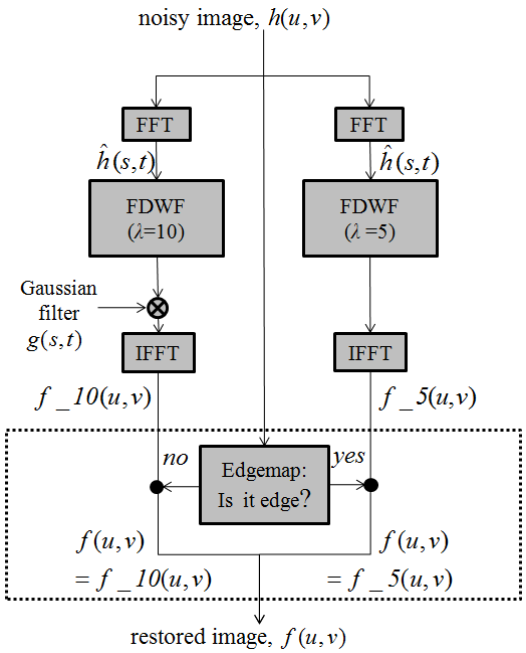

Fig.3 Block diagram of proposed method.

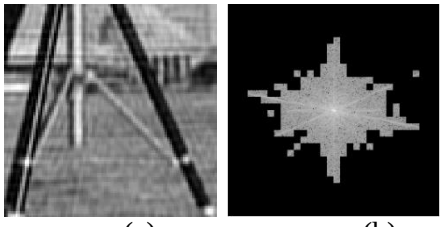

(a) (b)

Fig.4 Restored Cameraman and its logarithmic power spectrum (σ=25) by using FDWF (λ =10).

selected by visual effects evaluation. From the investigation, λ is set to 10. From Fig.4 we can observe that the noise level has been effectively reduced since noise is mostly cut out. On the other

hand, the image is blurred since the edges in higher frequencies are cut out as well. Obvious ringing effects can be observed in the restored image, which is caused by the sharp cutoff of the threshold range's edges in the frequency domain. When the image is inverted into the spatial domain, it generates decreasing oscillations as it progresses outward from the center. Narrower threshold range results in stronger oscillations.

To overcome the ringing effects, we multiply the output power spectrum filtered by the Wiener filter with a Gaussian lowpass filter, $g(s,t)$, to soften the threshold edges. The restored image is inverse-transformed to the spatial domain and denoted as $f\_10(u,v)$. In Fig.5, the ringing effects as seen in Fig.4 are successfully suppressed. From our investigation, the best parameter settings for the Gaussian lowpass filter are fixed to the size of 128×128 with the standard deviation of 10.

3.3 Edgemap Construction

Next, the decomposition of the smooth and non-smooth regions is performed pixel-by-pixel based on an edgemap. The edgemap is constructed by executing edge detection directly from the noisy image in the spatial domain. Although there is no pre-filtering process, the edges have been successfully obtained by using the proposed edge detection method. Another advantage of this technique is that it requires minimum parameter setting, which is only the sub-block size for the image division. The process of the edgemap construction is as follows.

First, the noisy image is divided into $k\times k$ non-overlapping sub-blocks (k=32), each of which consists of 8×8 pixels. Next, the pixel value range, $r_{(i,j)}(u,v)$, of each block (i,j: 1, 2, …, k) is calculated as

$$r_{(i,j)}(u,v)=\left|(r\_max-r\_min)/2\right| \tag{8}$$

where r_max and r_min are the maximum and minimum values of the pixels in the corresponding sub-block, respectively. Then, the $r_{(i,j)}(u,v)$ that represents the minimum value of the entire $r_{(i,j)}(u,v)$, denoted as R, is determined by

$$R=\min(r_{(i,j)}(u,v)). \tag{9}$$

This sub-block is assumed to be homogeneous and represents the smooth region. Thus, any pixel larger than R is considered as the non-smooth region. In order to determine whether a pixel in the

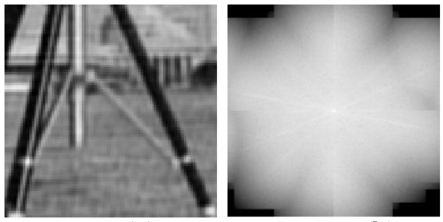

(a) (b)

Fig.5 Result for restored Cameraman (σ=25) by using FDWF (λ =10) multiplied with Gaussian lowpass filter.

(a) horizontal (b) vertical (c) 45°

(d) −45° (e) *edgemap*(u,v) (f) noisy Lenna

Fig.6. Edgemap constructions in four directions and combined edgemap for noisy Lenna (σ=25)

non-smooth region belongs to a line along the edges or additive noise, we consider the corresponding pixel and its two neighbouring pixels. If either difference of the (u,v)th pixel and its neighbouring pixels is larger than R, this pixel is considered as a part of a line along the edges. If both differences are lower than R, the corresponding pixel is assumed isolated from other non-smooth region's pixel, and considered as noise. The edge detection along a direction can provide a more precise distinction between edges and noise in noisy environments because isolated pixels can be detected easier. The edge detection is performed in four directions; (a) horizontal, $dh(u,v)$, (b) vertical, $dv(u,v)$, (c) 45°, $d45(u,v)$, and (d) −45°, $dm45(u,v)$.

$$dh(u,v)=\begin{cases}1= |h(u\text{-}1,v)\text{-}h(u,v)|>R \text{ or } |h(u,v)\text{-}h(u+1,v)|>R \\ 0 \quad \text{else}\end{cases} \tag{10}$$

$$dv(u,v)=\begin{cases}1= |h(u,v\text{-}1)\text{-}h(u,v)|>R \text{ or } |h(u,v)\text{-}h(u,v+1)|>R \\ 0 \quad \text{else}\end{cases} \tag{11}$$

$d45(u,v)=$

$$\begin{cases} 1 = |h(u+1,v-1)-h(u,v)|>R \text{ or } |h(u,v)-h(u-1,v+1)|>R \\ 0 \quad else \end{cases} \tag{12}$$

$$dm45(u,v)= \begin{cases} 1 = |h(u-1,v-1)-h(u,v)|>R \text{ or } |h(u,v)-h(u+1,v+1)|>R \\ 0 \quad else \end{cases}. \tag{13}$$

As can be observed from Fig. 6 ((a)-(d)), the edges have been successfully detected from different directions, regardless of the high noise level (see Fig. 6(f)). However, the edge detection from only a single direction is not sufficient to represent all the edges for the entire image. Thus, we suggest combining the edge detections of all four directions for better result. The combined edgemap, $edgemap(u,v)$, is constructed by

$$edgemap(u,v)= \begin{cases} 1 \quad dh(u,v) \text{ or } dv(u,v) \text{ or } d45(u,v) \text{ or } dm45(u,v)>0 \\ 0 \quad else \end{cases} \tag{14}$$

Fig.6(e) shows the edge detection of the $edgemap(u,v)$. Note that the $edgemap(u,v)$ provides relatively better edge detection along the lines in comparison with that of the single direction edge detection.

3.4 Edgemap-Based Image Restoration

The final restored image, $f(u,v)$, is constructed based on the edgemap as

$$f(u,v)= \begin{cases} f\_10(u,v) & edgemap(u,v)=0 \\ f\_5(u,v) & edgemap(u,v)=1 \end{cases}. \tag{15}$$

If the $edgemap(u,v)$ is equal to 0, then the (u,v)th pixel of the final restored image $f(u,v)$ is assumed as the smooth region, and assigned with the (u,v)th pixel value of $f\_10(u,v)$. Otherwise, $f(u,v)$ is assigned with those of $f\_5(u,v)$.

4 Results and Discussion

We have tested our method on nine grayscale test images (256×256) from the SIDBA database. All images are contaminated with additive Gaussian white noise (σ=5, 10, and 25). The Airplane, Girl, Lenna, Woman and Boat images represent smooth natural images. The Barbara, Building, Lighthouse and Text images represent natural images that are highly rich in both fine details and edges. We investigate the performances by using the mean measure of structural similarity (MSSIM) [9] since it is an image quality metric that well matches the human visual perception [9]. We also analyze the visual effects of the images. Each denoising method processes the test images with the same parameters setting (no tuning of parameters was performed for different noise level or image type).

We have compared our method to two Wiener filters in different domains: the LBWDWF [6] and FDWF [8] in blind condition. In this paper, the LBWDWF with 4 vanishing moments (db4) lifting-based wavelet transform utilizes 3 decomposition levels and 3 × 3 filtering window. The FDWF employs the setting as in Section 2. From Fig. 7(b)-(d) and Tables 1-3, our method clearly outperforms the other two methods over the entire range of noise levels. Our method is capable to reduce more noise compared to the FDWF and provides better preservation of the original image features than that of the LBWDWF.

Finally, we have also compared our method to two state-of-the-art methods: the ATV [1] and NLM [2]. They are reported to have significant performance in preserving details while eliminating the noise. Both denoising methods are performed in ideal condition, where the noise variances are known. Conversely, our method estimates the noise employing the approach as in Section 3. We perform the ATV based on the MATLAB code (default setting) as in [1]. In [2], the NLM suggested using the search window size of 21 × 21 and similarity window of 7× 7 for images with the size of 512× 512. However, the parameters setting as in [2] results in over-smoothed restored images for small resolution test image (256× 256). Thus, we set the search window and similarity window for the NLM to 5 × 5 and 2 × 2, respectively for better denoising results. From Tables 1-3, note that our method is better than the ATV in most cases. Our method is also better than the NLM in many images that are highly rich in both fine details and edges. In higher noise level, as can be seen in Fig. 7(d)-(f), the ATV and NLM result in strong noise removal. However, they eliminate the fine details and edges at the same time. Our method reduces considerable amount of noise and furthermore preserves fine details and edges better than the NLM and ATV. The investigation proves that our method with proposed noise estimation technique provides comparable performance with the state-of-the-arts methods performed in ideal condition. Table 4 shows the execution time for each denoising method implemented in MATLAB computed on a 1.4 GHz Intel Core 2 Duo CPU. The execution time of our method is slightly higher than that of the LBWDWF, but considerably lower if compared to that of the ATV and NLM.

5 Conclusion

From the study, it is found that our method is fast and more suitable for denoising images that are rich in both fine details and edges, especially in higher noise environments. The proposed edge detection technique is also capable to detect noise directly from the noisy image in any noise level, which has lead to an accurate decomposition of the smooth and non-smooth regions.

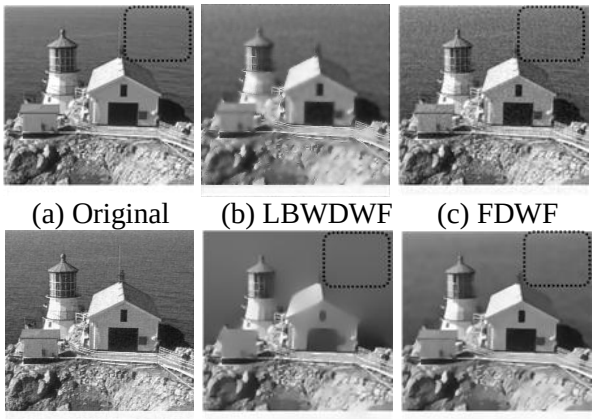

(a) Original (b) LBWDWF (c) FDWF

(d) Proposed (e) ATV (f) NLM

Fig. 7. Comparison of restored Lighthouse (high noise, σ=25).

Table 1.Performance comparison in MSSIM (σ=5)

Test images	LBW DWF (blind)	FD WF (blind)	Propo -sed (blind)	ATV (ideal)	NLM (ideal)
Barbara	0.67	0.95	0.96	0.94	0.97
Building	0.62	0.96	0.96	0.96	0.96
Lighthouse	0.68	0.91	0.94	0.90	0.93
Text	0.68	0.95	0.96	0.95	0.93
Airplane	0.81	0.89	0.92	0.95	0.94
Girl	0.82	0.91	0.92	0.91	0.93
Lenna	0.83	0.91	0.94	0.96	0.96
Woman	0.81	0.91	0.94	0.95	0.95
Boat	0.79	0.93	0.94	0.93	0.96

Table 2.Performance comparison in MSSIM (σ=10)

Test images	LBW DWF (blind)	FD WF (blind)	Propo -sed (blind)	ATV (ideal)	NLM (ideal)
Barbara	0.66	0.88	0.90	0.90	0.93
Building	0.62	0.89	0.91	0.90	0.91
Lighthouse	0.67	0.80	0.86	0.90	0.89
Text	0.68	0.88	0.89	0.90	0.88
Airplane	0.80	0.77	0.85	0.92	0.91
Girl	0.81	0.83	0.87	0.81	0.89
Lenna	0.82	0.82	0.88	0.92	0.92
Woman	0.80	0.82	0.87	0.90	0.91
Boat	0.78	0.84	0.88	0.86	0.92

Table 3.Performance comparison in MSSIM (σ=25)

Test images	LBW DWF (blind)	FD WF (blind)	Propo - sed (blind)	ATV (ideal)	NLM (ideal)
Barbara	0.66	0.82	0.85	0.41	0.84
Building	0.61	0.84	0.84	0.56	0.76
Lighthouse	0.66	0.72	0.79	0.75	0.79
Text	0.67	0.82	0.84	0.72	0.80
Airplane	0.78	0.70	0.78	0.58	0.86
Girl	0.80	0.77	0.81	0.55	0.82
Lenna	0.81	0.75	0.84	0.5	0.86
Woman	0.79	0.75	0.83	0.47	0.84
Boat	0.76	0.77	0.82	0.52	0.84

Table 4. Average time execution (s)

Noise, σ	LBW DWF	FD WF	Propo sed	ATV	NLM
5	0.60	0.31	0.93	23.33	67.31
10	0.56	0.31	0.92	66.17	68.60
25	0.57	0.30	0.93	751.49	67.82

References:

[1] G. Gilboa, N. Sochen, and Y. Zeevi, Texture preserving variational denoising using an adaptive fidelity term, *Proc. IEEE Workshop Variational and Level Set Methods in Computer Vision*,pp.137-144,2003. http://visl.technion. ac. il/~gilboa/PDE-filt/demo.adap.tv.m.

[2] A. Buades, B. Coll, and J.M. Morel, A non-local algorithm for image denoising, *Proc. IEEE Int. Conf. Computer Vision and Pattern Recognition*,vol.2,pp.60-65, 2005.

[3] N. Wiener, *Extrapolation, Interpolation, and Smoothing of Stationary Time Series*, Wiley, 1949.

[4] J. S. Lee, Digital image enhancement and noise filtering by use of local statistics, *IEEE Trans. Pattern Anal. Machine Intell.*, vol. PAMI-2, no.2,pp.165-168, 1980.

[5] H. Furuya, S. Eda, and T. Shimamura, Image restoration via Wiener filtering in the frequency domain, *WSEAS Trans. Signal Process.*, vol.5,no.2, pp.63-73, 2009.

[6] E. Ercelebi and S. Koc, Lifting-based wavelet domain adaptive Wiener filter for image enhancement, *IEE Proc. Vis. Image and Signal Processing*,vol.153,no.1,pp.31-36, 2006.

[7] L. Rudin, S. Osher, and E. Fatemi, Nonlinear total variation based noise removal algorithms, *Physica D*,vol.60,pp.259- 268,1992.

[8] S. Suhaila, and T. Shimamura, Power spectrum estimation method for image denoising by frequency domain Wiener filter, *Proc. IEEE Int. Conf. on Computer and Automation Engineering*, vol. 3,pp.608-612, 2010.

[9] Z. Wang, A. C. Bovik, H.R. Sheikh, and E. P. Simoncelli, Image quality assessment: from error visibility to structural similarity, *IEEE Trans. Image Process.*,vol.13,no.4,pp.600-612, 2004.